Environmental Science & Technology

Article

pubs.acs.org/est

Photochemistry of Dissolved Black Carbon Released from Biochar: Reactive Oxygen Species Generation and Phototransformation

Heyun Fu,[†] Huiting Liu,[†] Jingdong Mao,[‡] Wenying Chu,[‡] Qilin Li,[§] Pedro J. J. Alvarez,[§] Xiaolei Qu,*[,†] and Dongqiang Zhu[†]

[†]State Key Laboratory of Pollution Control and Resource Reuse, School of the Environment, Nanjing University, Nanjing, Jiangsu 210023, China

[‡]Department of Chemistry and Biochemistry, Old Dominion University, Norfolk Virginia 23529, United States

[§]Department of Civil and Environmental Engineering, Rice University, Houston Texas 77005, United States

Supporting Information

ABSTRACT: Dissolved black carbon (BC) released from biochar can be one of the more photoactive components in the dissolved organic matter (DOM) pool. Dissolved BC was mainly composed of aliphatics and aromatics substituted by aromatic C−O and carboxyl/ester/quinone moieties as determined by solid-state nuclear magnetic resonance. It underwent 56% loss of absorbance at 254 nm, almost complete loss of fluorescence, and 30% mineralization during a 169 h simulated sunlight exposure. Photoreactions preferentially targeted aromatic and methyl moieties, generating CH_2/CH/C and carboxyl/ester/quinone functional groups. During irradiation, dissolved BC generated reactive oxygen species (ROS) including singlet oxygen and superoxide. The apparent quantum yield of singlet oxygen was 4.07 ± 0.19%, 2−3 fold higher than many well-studied DOM. Carbonyl-containing structures other than aromatic ketones were involved in the singlet oxygen sensitization. The generation of superoxide apparently depended on electron transfer reactions mediated by silica minerals in dissolved BC, in which phenolic structures served as electron donors. Self-generated ROS played an important role in the phototransformation. Photobleaching of dissolved BC decreased its ability to further generate ROS due to lower light absorption. These findings have significant implications on the environmental fate of dissolved BC and that of priority pollutants.

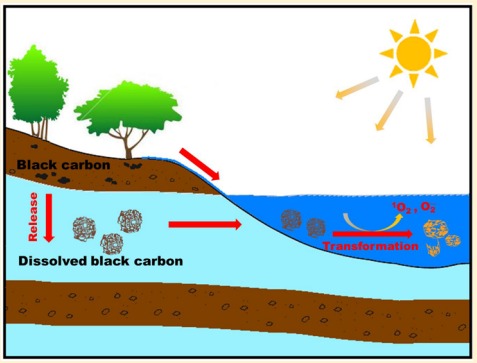

INTRODUCTION

Black carbon (BC) is the refractory carbonaceous residue generated from incomplete combustion of biomass and fossil fuel. Owing to its massive annual production and recalcitrant nature, BC plays a key role in the global carbon budget.[1,2] Dissolved BC, which is the water-soluble fraction of BC, can be readily mobilized from soils by infiltration and surface runoff. Globally, dissolved BC accounts for 10% of the riverine flux of dissolved organic carbon, being an important terrestrial BC input to oceans.[3] It comprises 5−7% of coastal oceanic dissolved organic matter (DOM) and >2% of oceanic DOM.[4,5] The photochemistry of DOM has been extensively studied and was found to be important in many aspects of aquatic environmental chemistry.[6] As an important constituent of the DOM pool,[3−5] the photochemistry of dissolved BC is expected to be important for understanding its own fate and that of priority pollutants.

A few studies have investigated the photochemistry of dissolved BC.[7−11] Dissolved BC in Congo River water (identified by Fourier transform ion cyclotron resonance mass spectrometry—FT-ICR MS) was more photolabile than other structural components in DOM, with an almost complete loss during a 57-day simulated sunlight irradiation.[7] Consistently, oceanic dissolved BC, as quantified by benzene poly(carboxylic acid) markers, was found to undergo photodegradation faster than oceanic colored DOM.[8] A recent study investigated the phototransformation/mineralization of dissolved and particulate BC released from biomass-derived BC (i.e., biochar).[9] The dissolved BC was more susceptible to phototransformation than particulate BC. The condensed aromatics in dissolved BC identified by FT-ICR MS were preferentially degraded during photoreactions, mainly yielding partially oxidized products. During sunlight exposure, the molecular weight distribution of dissolved BC shifted to lower ranges owing to the photodecomposition of high molecular weight fractions.[9,11] However, solar irradiation was found to induce the production of BC-like molecules from terrestrial DOM in the presence of iron.[10] This photochemical process potentially led to an annual flux of photoproduced BC to sediments equivalent to the flux of dissolved BC to the ocean. FT-ICR MS analysis provided the molecular masses and

Received: September 5, 2015
Revised: December 3, 2015
Accepted: December 30, 2015
Published: December 30, 2015

DOI: 10.1021/acs.est.5b04314
Environ. Sci. Technol. 2016, 50, 1218−1226

allowed the comparison of compound types in different dissolved BC samples. However, this technique is qualitative to semiquantitative due to the large variation in ionization efficiencies of different molecules.[12] Our understanding of the quantitative structural changes of dissolved BC during solar irradiation and the underlying mechanism is still limited. Solid-state nuclear magnetic resonance (NMR) is a suitable technique for quantitative investigations of the DOM structure. However, it has not been used to study the phototransformation of dissolved BC. Reactive oxygen species (ROS) are highly reactive phototransients which promote the indirect photodegradation/transformation of organic contaminants and DOM.[6,13] To date, the ability of dissolved BC to generate ROS is still unknown.

In the present study, we investigated the phototransformation process of dissolved BC leached from bamboo biomass-derived biochar under simulated sunlight and its ability to generate ROS. Our objectives were to (1) quantify the photoinduced structural changes of dissolved BC, and (2) characterize ROS generation by dissolved BC and the role of self-generated ROS in the phototransformation process. To the best of our knowledge, this is the first study to evaluate ROS generation of dissolved BC and to provide quantitative information regarding its photoinduced structural changes using ^{13}C solid-state NMR.

MATERIALS AND METHODS

Materials. Furfuryl alcohol (FFA, 98%), 2,3-bis(2-methoxy-4-nitro-5-sulfophenyl)-2*H*-tetrazolium-5-carboxanilide (XTT, > 90%), sodium borohydride ($NaBH_4$, > 98%), terephthalic acid (TPA, 98%), sodium azide (>99.5%), phenol (>99%), and superoxide dismutase (SOD, from bovine erythrocytes) were purchased from Sigma-Aldrich, U.S.A. Deuteroxide (D_2O, 99.8 atom % D) was purchased from Tokyo Chemical Industry, Japan. Deionized water (18.2 MΩ·cm resistivity at 25 °C) produced by an ELGA Labwater system (PURELAB Ultra, ELGA LabWater Global Operations, U.K.) was used in all the experiments.

Preparation of Dissolved BC. BC was prepared from bamboo shavings collected from Lishui, Zhejiang Province, China. The biomass was pulverized into fine powder using a high-speed pulverizer (FW 100, Tianjin Taisite Instrument, China) and pyrolyzed in a muffle furnace under oxygen-limited conditions. The pyrolysis temperature was programed to increase from 20 to 400 °C in 2 h and maintain at 400 °C for another 3 h. The resulting BC was further ground to pass a 100-mesh sieve. Our previous study suggests that dissolved BC can be readily released from bulk BC by stirring in water.[14] 30 g BC was mixed with 500 mL deionized water in a 1000 mL glass beaker. The mixture was sonicated in a bath sonicator (KH-800TDB, Kunshan Hechuang Ultrasonic Instrument, China) at 100 W for 30 min to achieve the extensive release of dissolved BC. It was then filtered through 0.45-μm membranes (Pall, U.S.A.). The residue retained on the membrane was collected and subjected to another round of sonication and filtration. After three cycles of sonication extraction, dissolved BC solution (i.e., the filtrate passing through 0.45-μm membranes) was collected and freeze-dried. The resulting dissolved BC powder was stored in a desiccator at room temperature prior to use.

Part of the dissolved BC was demineralized using a previous described procedure.[15] Briefly, dissolved BC powder was treated with 1 M HCl and 1 M HF mixture (w:v, 1:10) for 4 h and neutralized with 1 M NaOH. The residual salts were removed by dialysis using dialysis bags (1000 Da, Union Carbide, U.S.A.).[16] The demineralization procedure was repeated twice and the resulting sample was freeze-dried and harvested as demineralized dissolved BC. To probe the role of carbonyl-containing structures in the photochemistry of dissolved BC, reduction reaction was carried out using $NaBH_4$ to reduce carbonyl groups of aliphatic and aromatic ketones/quinones to alcohols, phenols, and hydroquinones[17] based on procedure modified from a previous study.[18] 50 mL of 400 mg/L dissolved BC was sparged with N_2 for 30 min. $NaBH_4$ was added into the solution at a mass ratio of $NaBH_4$/dissolved BC = 10:1. The mixture was stirred at 200 rpm and sparged with N_2 for 3 h. Then, the pH of the solution was lowered to 5.0 using HCl and sparged with air for 1 h to quench the excess $NaBH_4$. The resulting sample was diluted to 200 mg/L, adjusted to pH 7.0, and stored overnight before the experiments.

Photochemical Experiments. Production of $^1O_2$, O_2^-, and ·OH was quantified using probe molecule FFA, XTT, and TPA, respectively. For most experiments, 100 mL of 100 mg/L dissolved BC solution (corresponding to 14.46 mg C/L) with a respective probe molecule was magnetically stirred at 200 rpm in a 250 mL cylindrical quartz cell equipped with a water-circulating jacket. The reaction temperature was maintained at 20 ± 0.1 °C by a water circulating temperature control system (DC0506, Shanghai FangRui Instrument Co., Ltd., China). The solutions were irradiated from the top by a xenon lamp (CEL-HXF300, AULTT, China) with an output energy of 50 W at a distance of 0.2 m (see Figure S1a for the details about experimental setup). The lamp spectrum was collected using a spectrometer USB2000+ (Ocean Optics, FL, U.S.A.), which was similar to that of natural sunlight (Figure S1b). The irradiation energy at the water surface was 25.3 mW/cm^{-2} in the range of 290−400 nm, equivalent to 5.8 sun power.[19] Sample aliquots of 0.5 mL were withdrawn periodically from the reactor during the irradiation for analysis. The solution pH was 7.2 ± 0.3 without any adjustment. Solutions containing ROS probe molecules without dissolved BC were irradiated under the same condition as blank controls. Experiments were also carried out in the dark as dark controls. For experiments using demineralized and photobleached dissolved BC, ROS measurements were conducted in a 40 mL glass bottle with 20 mL of 30 mg/L demineralized dissolved BC solution (corresponding to 14.38 mg C/L, at pH of 6.95) or 100 mg/L photobleached dissolved BC which was immersed in a water-circulating bath at 20 ± 0.1 °C. A parallel sample with 20 mL of 100 mg/L original dissolved BC was irradiated at the same experiment conditions for comparison. A summary of experimental conditions can be found in Table S1.

Singlet oxygen ($^1O_2$) formation was quantified by monitoring the loss of FFA as described previously.[20,21] FFA was added to dissolved BC solutions at an initial concentration of 0.2 mM. During the irradiation, the remaining FFA in the solutions was measured using an HPLC (Agilent 1100, Agilent Technologies, U.S.A.) with a Zorbax Eclipse SB-C18 column (Agilent) and the detection wavelength was 220 nm. The mobile phase was 30% acetonitrile/70% 0.1 wt % phosphoric acid. The steady-state concentration and apparent quantum yield of $^1O_2$ was determined according to previously reported methods (see details in the Supporting Information, SI).[22] The formation of XTT formazan from XTT (at an initial concentration of 0.05 mM) was used to quantify superoxide (O_2^-).[23,24] XTT

DOI: 10.1021/acs.est.5b04314
Environ. Sci. Technol. 2016, 50, 1218−1226

formazan was measured using a UV-6100 double beam spectrophotometer (Mapada, China) at 475 nm. The extinction coefficient of XTT formazan is 23800 $M^{-1}cm^{-1}$.[24] The loss of TPA was used to quantify the production of hydroxyl radical (·OH).[25] TPA stock solution was made in 2 mM NaOH and filtered through a 0.45-μm membrane. The initial concentration of TPA in the dissolved BC solutions was 0.5 mM. The concentration of TPA was quantified by HPLC using a mobile phase of 30% acetonitrile/70% 0.1 wt % phosphoric acid and detection wavelength of 254 nm.

Phototransformation Experiments. Phototransformation experiments were carried out in the same irradiation setup as described above. 100 mL of 100 mg/L dissolved BC was exposed to the simulated sunlight in a 250 mL cylindrical cell at 20 °C. The phototransformation kinetics of dissolved BC was monitored by UV−vis and fluorescence spectroscopy. The absorption spectral slopes, $S_{275-295}$ and $S_{350-400}$, and slope ratios, S_R, were calculated according to the procedure described in a previous study.[26] The fluorescence excitation−emission matrix (EEMs) spectrum was collected on a F-7000 fluorescence spectrophotometer by scanning excitation wavelengths from 200 to 600 nm and detecting the emission fluorescence between 200 and 600 at 5 nm interval. The photomineralization kinetics was examined by total organic carbon (TOC) measurements (multi N/C 3100, ANALYTIKJENA, Germany). To explore the role of self-generated ROS in the photochemical transformation of dissolved BC, ROS scavengers including sodium azide and SOD were used to quench specific ROS in the inhibition experiments. D_2O was used to probe the role of $^1O_2$ by extending its lifetime.

NMR Analysis. For solid-state NMR analysis, 100 mL of 1000 mg/L dissolved BC was irradiated in a 250 mL cylindrical cell at 20 °C for 288 h (12 days). The original and irradiated dissolved BC were both freeze-dried and characterized by quantitative ^{13}C multiple Cross-Polarization/Magic Angle Spinning (multiCP/MAS) NMR. The NMR spectra were acquired on a Bruker AVANCE III 400 NMR spectrometer (Bruker, Massachusetts, U.S.A.) at a spinning speed of 14 kHz and a 90° ^{13}C pulse-length of 4 μs. The nonprotonated and mobile carbon in dissolved BC was further differentiated using multiCP/MAS with recoupled dipolar dephasing technique (multiCP/MAS/DD).[27,28] The recycle delay was set to be 0.5 s and the dipolar dephasing time was 60 μs.[28]

RESULTS AND DISCUSSION

Dissolved BC Underwent Phototransformation under Simulated Sunlight. The phototransformation kinetics of dissolved BC under simulated sunlight was monitored using UV−vis and fluorescence spectrometers (Figure 1 and 2). Sunlight irradiation led to a decrease in absorbance with increasing exposure time over the entire range of the UV spectrum (Figure 1a). The phototransformation kinetics was examined by plotting the absorbance at 254 nm (A_{254}) as a function of exposure time (Figure 1b). The A_{254} decreased with increasing exposure time, with a 56% reduction in 169 h. The phototransformation followed first-order kinetics (R^2 = 0.97). The pseudo-first-order model reaction rate constant was 3.7 × 10^{-3} h^{-1} (half-life of 187 h). Spectral ratios, spectral slopes, and slope ratios were often used to interpret structural information from the UV−vis spectra of DOM and were tentatively used for dissolved BC (Figures S2−S6). The E_2/E_3 of dissolved BC (i.e., the UV absorbance at 254 nm divided by that at 365 nm) gradually increased from 5.47 to 11.69 during 169 h irradiation

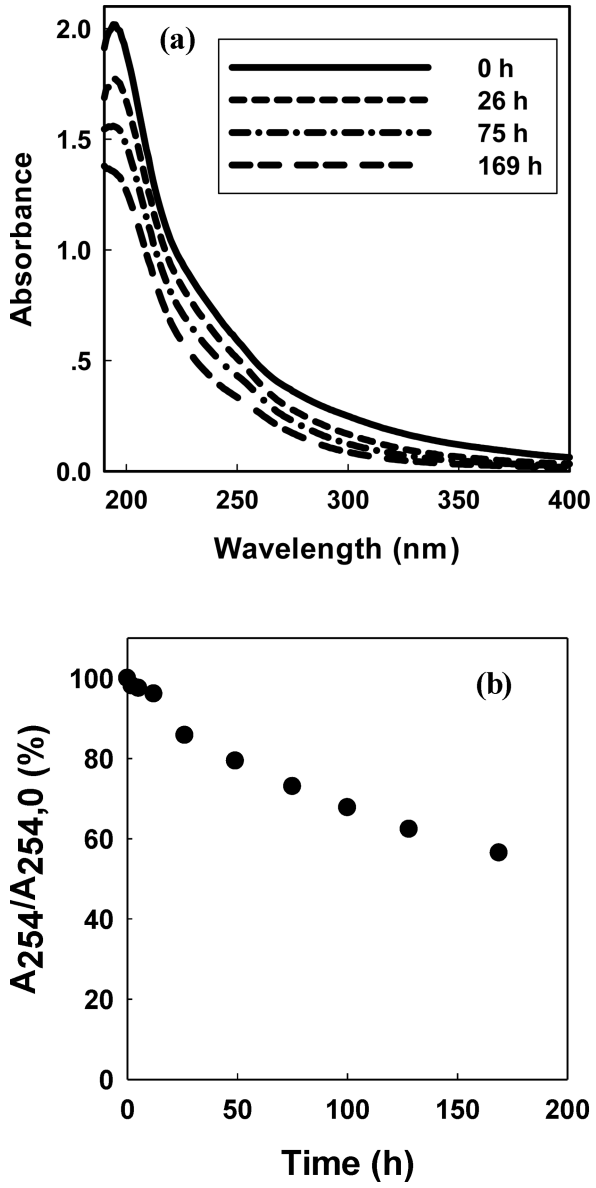

Figure 1. (a) UV spectra of 100 mg/L dissolved BC under simulated sunlight irradiation and (b) phototransformation kinetics of 100 mg/L dissolved BC monitored by absorption at 254 nm.

(Figure S2). Meanwhile, the slope ratio of dissolved BC, S_R, increased from 1.14 to 2.40 (Figure S5). The overall trend of E_2/E_3 and S_R collectively indicated that the colored components in dissolved BC changed from high molecular weight compounds to low molecular weight compounds.[26,29,30] This is in agreement with previous studies on the photobleaching of DOM.[9,26,31] The E_4/E_6 ratios (the ratio of absorption at 465 to 665 nm) of dissolved BC was found to decrease with irradiation time, indicating the decrease of its aromaticity (Figure S6).[32]

The original EEM spectrum of dissolved BC had a strong peak at excitation/emission wavelength pair of E_x 320 nm/E_m 420 nm, which is commonly associated with the presence of humic acid-like compounds (Figure 2a).[33] This peak was also found in the EEM spectra of dissolved BC derived from a biomass mixture of tealeaf willow and feather moss.[9] The EEM spectra of dissolved BC observed here were simpler than that of common DOM which often contained peaks in several EEM

DOI: 10.1021/acs.est.5b04314
Environ. Sci. Technol. 2016, 50, 1218−1226

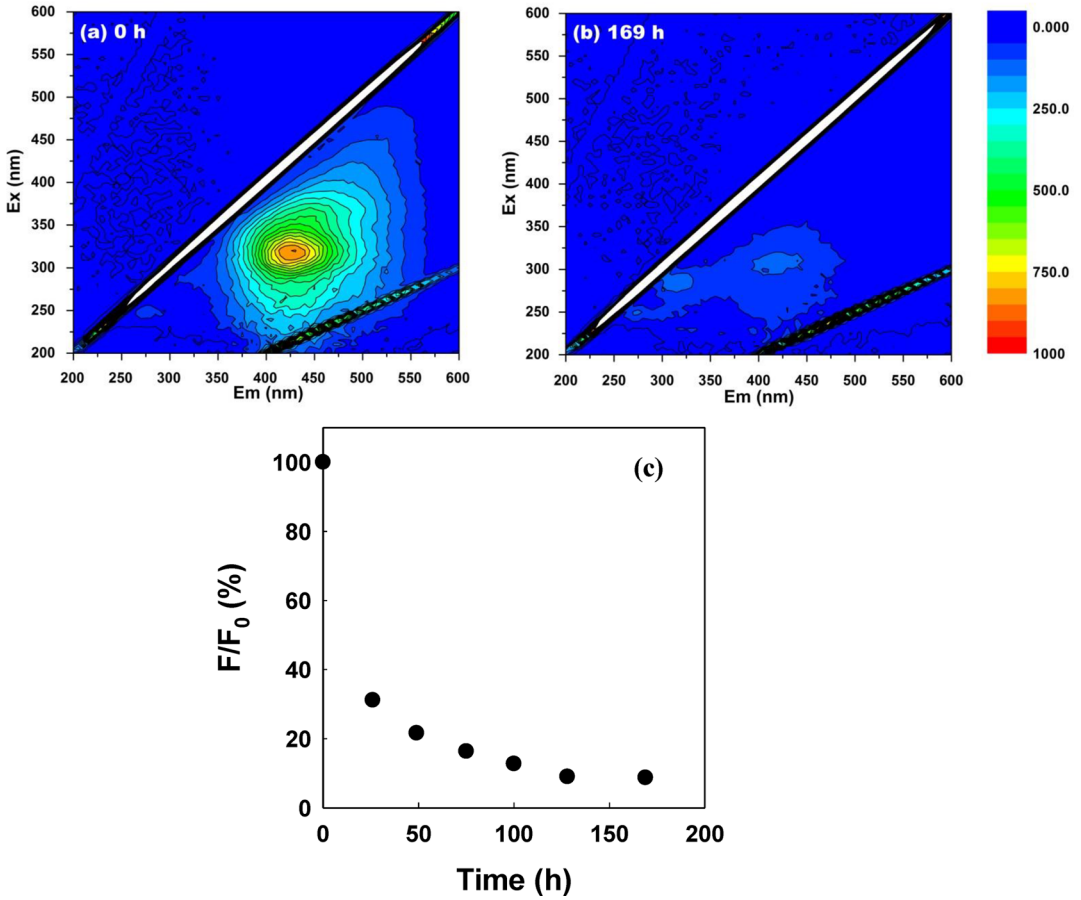

Figure 2. Fluorescence excitation emission matrices of 100 mg/L dissolved BC (a) before and (b) after 169 h simulated sunlight irradiation; and (c) phototransformation kinetics of 100 mg/L dissolved BC monitored by E_x/E_m 320 nm/420 nm.

regions,[33] indicating its less complex fluorophore components. Figure 2b clearly shows that the original fluorescence was almost completely removed after 169 h irradiation. The intensity of the EEM peak reduced with increasing irradiation time, with a sharp decrease in the first 26 h and a 96% reduction in 169 h (Figure 2c). The half-life of the phototransformation of dissolved BC determined by fluorescence indicators was about 19 h, much shorter than that determined by UV−vis indicators. Similarly, previous studies suggested that the fluorescent fulvic and humic aromatic structures of various DOM were preferentially degraded under solar irradiation.[34] Meanwhile, only 30% of dissolved BC was found to be mineralized during 169 h irradiation as indicated by the TOC measurements (Figure S7). Thus, dissolved BC mainly underwent phototransformation rather than complete photomineralization under sunlight, in line with previous findings.[9]

Structure of Dissolved BC was Significantly Altered by Simulated Sunlight Exposure. Structural changes of dissolved BC during the simulated sunlight exposure were investigated using quantitative solid-state ^{13}C multiCP/MAS/DD NMR (Figure 3). The spectrum of dissolved BC contained sharp and well-resolved peaks, which were different from the broad bands in the spectra of DOM caused by the overlay of signals from various moieties, indicating its relative simple structure (Figure 3a). The spectrum was separated into following regions:[35] 7−22 ppm, methyl; 22−50 ppm, CH_2, CH, or C in aliphatics; 50−90 ppm, O- or *N*-alkyl; 90−150 ppm, aromatic carbon; 150−165 ppm, aromatic C−O in phenolic or aromatic C−O−C groups; 165−190 ppm, C=O in N−C=O, carboxyl, ester, or quinone; 190−220 ppm, C=O in ketone, quinone, or aldehyde. The composition of functional moieties in dissolved BC samples as determined by NMR were summarized in Table 1. The peaks at 18.8 and 25.2 ppm were assigned to CH_3 groups and $-(CH_2)_n-$ moieties. These moieties were mobile/flexible as their signals were preserved after recoupled dipolar dephasing.[36] The peak at 128.3 ppm was the characteristic signal of aromatic rings. It is worth noting that as there was little signal of NCH (44−64 ppm) of amide[35] in the spectrum, the bonds between 165 and 190 ppm should be ascribed to C=O in carboxyl/ester/quinone. The peaks at 180.2 ppm might represent the carboxyls. There was little signal in the 50−90 ppm and 190−220 ppm regions, suggesting minimal presence of O/*N*-alkyl, ketone, or aldehyde structures in dissolved BC. Thus, the original dissolved BC was mainly comprised of aromatics substituted by aromatic C−O moieties and C=O in carboxyl/ester/quinone, as well as mobile/flexible aliphatics.

After irradiation, the structure of dissolved BC changed substantially (Figure 3b, Table 1). The aromatic carbon in dissolved BC reduced from 43.7% to 35.0%, leading to the decrease of the aromaticity (aromatic and aromatic C−O carbon) from 49.2% to 40.9%. This was in line with the E_4/E_6 data of the UV−vis spectra. The peak for methyl at 18.8 ppm was eliminated after irradiation. However, CH_2/CH/C in aliphatics increased from 15.1% to 20.4%; aromatic C−O slightly increased from 5.5% to 5.9%; and C=O in carboxyl/ester/quinone increased from 32.4% to 35.8%. The multiCP/

DOI: 10.1021/acs.est.5b04314
Environ. Sci. Technol. 2016, 50, 1218−1226

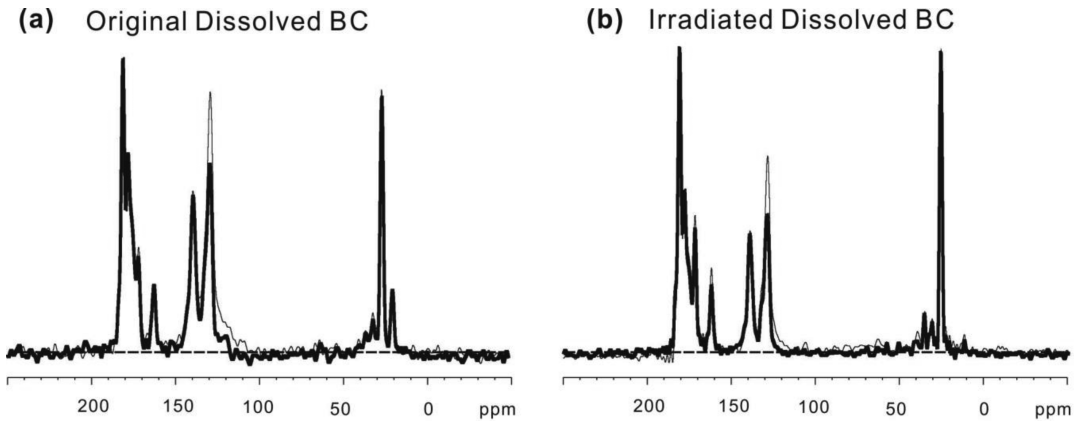

Figure 3. Quantitative solid-state ^{13}C multiCP/MAS NMR sepctra (thin lines) and multiCP/MAS after recoupled dipolar dephasing (thick lines) of dissolved BC samples (a) before and (b) after 288 h simulated sunlight irradiation.

Table 1. Composition of Functional Groups (in % of total C) in Dissolved BC Obtained by Quantitative ^{13}C multiCP/MAS NMR[a]

	7−22	22−50	50−90	90−150		150−165	165−190	190−220
				aromatic	aromatic			
moieties location (ppm)	CH_3	CH_2/CH/C	O/*N*-alkyl	C−C	CH	aromatic C−O	carboxyl/ester/quinone	ketone/quinone/aldehyde
original dissolved BC	3.4	15.1	N.D.	29.0	14.7	5.5	32.4	N.D.
irradiated dissolved BC	2.9	20.4	N.D.	25.8	9.2	5.9	35.8	N.D.

[a]N.D. represents non-detectable.

MAS/DD spectrum suggests that the original dissolved BC contained 14.7% protonated aromatic carbon, while the irradiated sample only contained 9.2%. This was caused by both the substitution of carboxyl/ester/quinone groups on the aromatic rings and the ring cleavage. The nonprotonated aromatic carbons also decreased from 29.0% to 25.8%, indicating the breakdown of aromatic regions. These results suggest that photoreactions preferentially degraded aromatic structures and methyl groups, generating CH_2/CH/C in aliphatics, and C=O in carboxyl/ester/quinone. The preferential degradation of aromatics was qualitatively consistent with previous DOM studies using FT-ICR MS technique.[7,9,37] The result was also generally in line with an X-ray absorption spectroscopy study which suggested that DOM lost aromatic/unsaturated carbon and gained carboxyl and O-alkyl carbon during solar irradiation in the presence of iron.[10] It was consistent with our UV−vis and fluorescence data as many chromophores and fluorophores contain aromatic structures.[38] The increase of aliphatics can be attributed to both the selective preservation and the generation of new aliphatics. Helms et al. suggested that the alkyl structures in DOM were resistant to both direct and indirect photodegradation.[31] Our data indicate that among alkyl structures, the methyl was preferentially degraded. Other alkyls were either relatively resistant to photodegradation or produced in photoreactions which compensated their loss. Photoproduced aliphatics were previously identified during the phototransformation of DOM,[31] while its origin was not clear. Our data suggest that new CH_2/CH/C could be generated from the oxidation of methyl groups and the cleavage of aromatics.

Dissolved BC Efficiently Produced $^1O_2$ and O_2^- under Simulated Sunlight. The ROS generated by dissolved BC was quantified using probe molecules. Figure 4a presents the FFA concentration, the $^1O_2$ probe, as a function of irradiation time. FFA was stable in dark as well as under sunlight without dissolved BC. Fast FFA degradation was observed in the presence of dissolved BC under sunlight, with a 93% loss in an 8-h period. The pseudosteady-state concentration, $[^1O_2]_{ss}$, was calculated to be $1.46 \pm 0.07 \times 10^{-12}$ M. The apparent quantum yield $\Phi_{\text{singlet oxygen}}$ was calculated to be 4.07 ± 0.19%. Meanwhile, the $\Phi_{\text{singlet oxygen}}$ for Suwannee River humic acid measured in this work was 1.57% (Figure S8), close to that reported in earlier studies.[39,40] The apparent quantum yield of dissolved BC was higher than that of many well-studied DOM, including Suwannee River humic acid (1.38 ± 0.08% and 1.60 ± 0.08%),[37,38] Suwannee River fulvic acid (1.85 ± 0.15% and 2.11 ± 0.31%),[39,40] Suwannee River natural organic matter (2.02 ± 0.23% and 1.81%),[22,40] Nordic aquatic humic acid (1.18%),[22] Nordic aquatic fulvic acid (2.03%),[22] Nordic DOM (2.48%),[22] and Pony lake fulvic acid (1.34 ± 0.09%).[39] Thus, dissolved BC is one of the more photoactive components in the DOM pool in terms of generating $^1O_2$.

Previous studies of DOM photochemistry suggested that $^1O_2$ production occurred through energy transfer from DOM triplets, ^{3}DOM*, to O_2.[22] Several studies suggested that there was a positive correlation between the E_2/E_3 ratio of DOM and its $\Phi_{\text{singlet oxygen}}$.[18,22,40] The E_2/E_3 of dissolved BC was 5.47, higher than commonly studied DOM (3.06−4.77).[40] The high E_2/E_3 of dissolved BC likely indicates its lower molecular weight as compared with other DOM[30] and consequently less intramolecular charge transfer,[22] resulting in enhanced quantum yield of ^{3}DOM* and consequently the higher $\Phi_{\text{singlet oxygen}}$. The $^1O_2$ generating chromophores in DOM were suggested to be mainly aromatic ketones, quinones, and aromatic amino acids.[18,41,42] The presence of aromatic amino acids in dissolved BC was minimal due to the lack of signals of NCH in amide (44−64 ppm)[35] in the NMR spectrum. To assess the role of carbonyl-containing structures in the generation of $^1O_2$, dissolved BC was treated with borohydride ($NaBH_4$) to preferentially reduce carbonyl-containing struc-

DOI: 10.1021/acs.est.5b04314
Environ. Sci. Technol. 2016, 50, 1218−1226

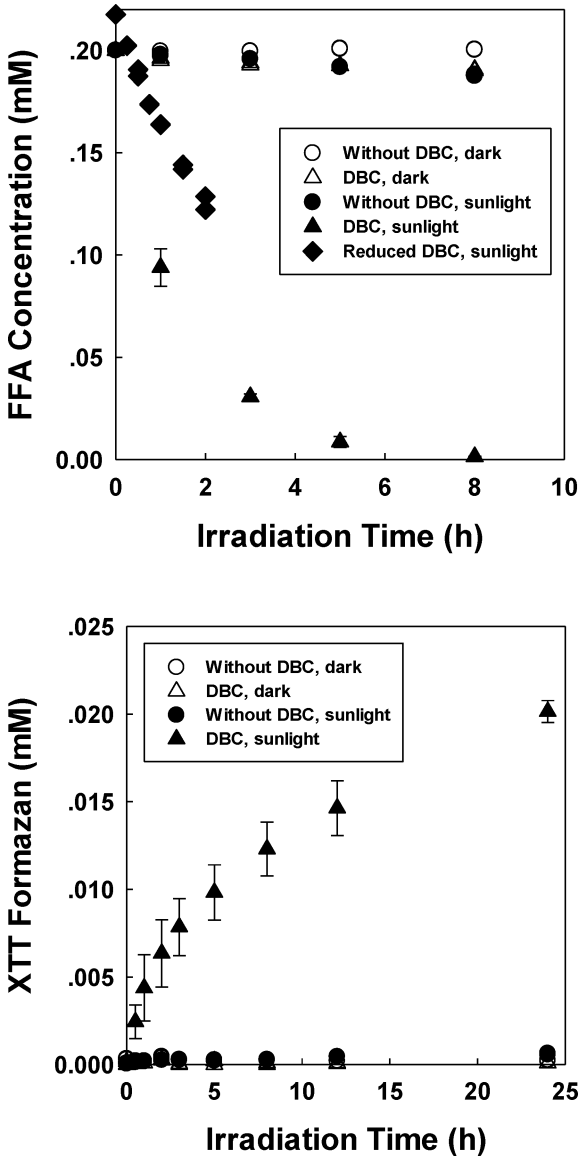

Figure 4. (a) FFA loss, representing $^1O_2$ generation, and (b) XTT formazan production, representing O_2^- generation as a function of irradiation time with and without 100 mg/L dissolved BC (DBC)/$NaBH_4$-reduced dissolved BC (reduced DBC) and simulated sunlight. Error bars represent ± one standard deviation from the average of triplicate tests.

tures of aliphatic and aromatic ketones/quinones to alcohols, phenols, and hydroquinones.[17,43] The reduced dissolved BC had lower absorbance than the original sample due to the destruction of charge transfer interactions within the molecules (Figure S9), consistent with earlier studies.[18,43] $NaBH_4$-treated dissolved BC generated less $^1O_2$ (Figure 4a). Its $\Phi_{singlet\ oxygen}$ was 3.18%, lower than the original dissolved BC. These results suggested that carbonyl-containing structures were involved in the generation of $^1O_2$. It is worth noting that aromatic ketones played a minimal role in this case due to the fact that dissolved BC had little aromatic ketones (Table 1). However, chromophores other than carbonyl-containing structures are also important as $NaBH_4$-treated dissolved BC still generate significant amount of $^1O_2$.

Figure 4b shows the formation of XTT formazan, which is the product of reactions between XTT and O_2^-, as a function of irradiation time. No XTT formazan was formed in dark conditions and under sunlight without dissolved BC. XTT transformation was observed in the presence of dissolved BC under sunlight, indicating the generation of O_2^-. The generation rate of O_2^- was 1.2×10^{-9} M s^{-1} in the first 3 h of the experiment ($R^2 = 0.99$). The generation of O_2^- by DOM is often attributed to the electron transfer between excited DOM and oxygen or the reduction of $^1O_2$ by electron donors in DOM.[22,44,45] In this work, the latter mechanism can be ruled out due to the fact that demineralized dissolved BC generated significant amount of $^1O_2$ but little O_2^- (Figure 5). The phenolic groups were previously identified as active moieties in DOM for O_2^- generation.[39] Dissolved BC contained significant amount of phenolic carbon as part of aromatic C—O moieties which could be responsible for O_2^- generation. However,

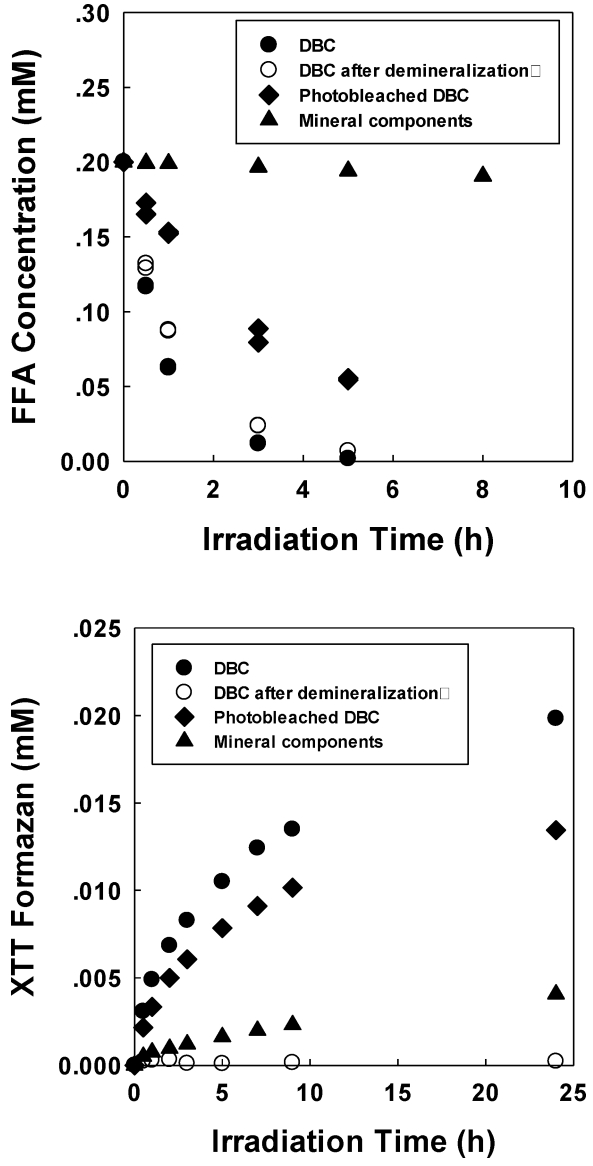

Figure 5. (a) FFA loss, representing $^1O_2$ generation, and (b) XTT formazan production, representing O_2^- generation as a function of irradiation time in the presence of 100 mg/L (14.38 mg C/L) dissolved BC (DBC), 14.46 mg C/L demineralized dissolved BC, 100 mg/L dissolved BC after 24 h sunlight irradiation (photobleached DBC), and 50 mg/L minerals under simulated sunlight.

DOI: 10.1021/acs.est.5b04314
Environ. Sci. Technol. 2016, 50, 1218−1226

phenol-like structures alone did not lead to O_2^- generation, which will be discussed in detail in the following section. There was no significant degradation of TPA, the ·OH probe, during 8 h of irradiation, indicating little ·OH formation by dissolved BC (Figure S10).

Elemental analysis suggests that our dissolved BC sample contained 48.2% minerals which could be involved in the ROS generation. The major elements in the minerals were potassium and silicon as determined by X-ray fluorescence measurement (Table S1). In order to further clarify this issue, demineralized dissolved BC was subjected to ROS generation tests. Figure 5 compares the ROS generation by dissolved BC, demineralized dissolved BC, photobleached dissolved BC, and organic-free minerals. The pseudo-first-order FFA degradation rate constants of demineralized and photobleached dissolved BC were normalized by the photon absorption ratio, $R_a/R_{a,\text{original dissolved BC}}$ (see details in the SI), to take account of changes of light absorption after the treatments. Demineralized dissolved BC generated significant amount of $^1O_2$. The normalized pseudo-first-order FFA degradation rate constant in demineralized dissolved BC solution was 0.43 h^{-1}, lower than that in original dissolved BC, 0.95 h^{-1}. However, no O_2^- formation was observed for demineralized dissolved BC. Thus, the minerals played two possible roles in the O_2^- generation: (1) the minerals could be photoactive and generated all O_2^-; or (2) the generation of O_2^- by dissolved BC depended on the synergy between the organic carbon and minerals. To further test these two hypotheses, organic-free minerals in dissolved BC were isolated by heat treatment of BC at 600 °C in air for 6 h which removed organic carbon. As shown in Figure 5, the minerals were photoactive, which could be attributed to its silica constituents.[25] They generated very small amount of $^1O_2$, but significant amount of O_2^-. However, the O_2^- generated by dissolved BC was much higher than the sum of demineralized dissolved BC and minerals, indicating a synergistic effect. We postulate that the minerals formed charge transfer complex ([D, A], [D]/electron donor, [A]/electron acceptor) with organic carbon, which enhanced the formation of ion radical pair, $[D^{\bullet+}, A^{\bullet-}]$, upon light irradiation. The rich phenol-like structures in organic carbon most likely served as [D];[41] and the minerals served as [A]. $[D^{\bullet+}, A^{\bullet-}]$ could further form charge separated pair $D^{\bullet+}$ and $A^{\bullet-}$, which subsequently transferred electrons to O_2 to form O_2^-. To test our hypothesis, phenol was used as a model electron donor to investigate the charge transfer process. Two new peaks at 235 and 288 nm were observed on the difference spectrum of the phenol–mineral mixture versus the sum of phenol and mineral spectra (Figure S11). These peaks had wavelengths longer than the characteristic absorbance of phenol (i.e., 209 and 270 nm), indicating the formation of charge transfer complex [D, A] between phenol and minerals. The mixture of 100 mg/L phenol and 50 mg/L minerals was then subjected to simulated sunlight exposure. The presence of phenol significantly enhanced the O_2^- generation by 19.6% ($p < 0.05$) as compared with minerals alone. This suggests that photoinduced electron transfer between the organic carbon and minerals in dissolved BC could be one of the O_2^- generation mechanisms as described in eqs 1–3:

$$[D, A] + h\nu \rightarrow [D^{\bullet+}, A^{\bullet-}] \quad (1)$$

$$[D^{\bullet+}, A^{\bullet-}] \rightarrow D^{\bullet+} + A^{\bullet-} \quad (2)$$

$$A^{\bullet-} + O_2 \rightarrow A + O_2^- \quad (3)$$

The ability of dissolved BC to generate ROS was affected by the phototransformation/mineralization process and the resulting structural changes. Dissolved BC after 24 h simulated sunlight exposure (i.e., photobleached dissolved BC) generated significantly less $^1O_2$ and O_2^- than the original sample as shown in Figure 5. The normalized pseudo-first-order FFA degradation rate constant in photobleached dissolved BC solution was 0.93 h^{-1}, similar to that in the original dissolved BC, 0.95 h^{-1}. Thus, the decreased ROS generation by photobleached dissolved BC could be mainly attributed to its lower light absorption.

Self-Generated ROS Played an Important Role in the Phototransformation. In order to further probe the role of self-generated ROS in the phototransformation process, inhibition experiments were carried out and the results were summarized in Figure 6. Ten mM sodium azide was used to scavenge $^1O_2$. The presence of sodium azide reduced the phototransformation by 10.8%, indicating the $^1O_2$-mediated oxidation of dissolved BC. In accord with this suggestion is the result of the irradiation test in D_2O. The phototransformation was enhanced by 24.3% in D_2O which increases the lifetime of $^1O_2$ due to the kinetic solvent isotope effect.[46] The interactions between $^1O_2$ and humic substances have been previously reported.[13,45] The reactions were suggested to mainly result in incorporation of O atoms into humic substances,[13,45] in line with the NMR data and the relatively small change of TOC during the irradiation. This is also consistent with a previous study which suggests that dissolved BC is partially oxidized during solar exposure, rather than photomineralized to CO_2.[9] The irradiation was then conducted in the presence of 5 mg/L SOD, a known scavenger of O_2^-. The phototransformation of dissolved BC was inhibited by 13.9%, indicating that O_2^- also mediated the oxidation of dissolved BC. It was reported that scavengers such as sodium azide were only efficient in quenching ROS in bulk solutions.[47] ROS in DOM macromolecules, which are more important in phototransformation

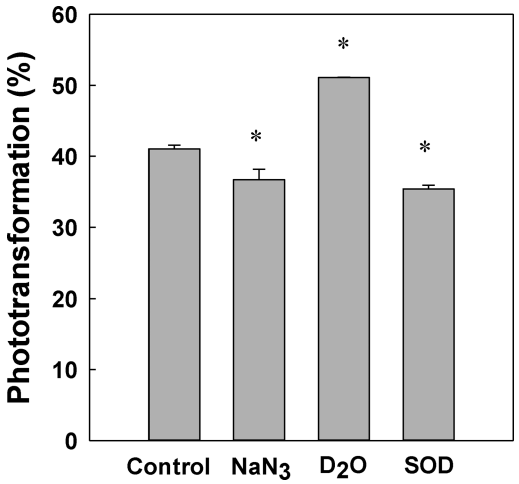

Figure 6. Phototransformation percentages of 100 mg/L dissolved BC under simulated sunlight in deionized water (control), 10 mM NaN_3, 90% D_2O, or 5 mg/L SOD after 24 h simulated sunlight exposure. Error bars represent standard deviation of triplicates. The phototransformation rates were quantified using the reduction of absorption at 300 nm. The * represents statistically different values from the control as tested by the Student's *t*-test ($p < 0.05$).

DOI: 10.1021/acs.est.5b04314
Environ. Sci. Technol. 2016, 50, 1218–1226

processes, are much higher than that in bulk solutions and less affected by scavengers.[47] Therefore, the contribution of self-generated ROS to the phototransformation of dissolved BC should be significant higher than that predicted based on the inhibition experiments.

Environmental Implications. Our results suggest that dissolved BC, as an important component of the BC continuum and the DOM pool, can efficiently generate $^1O_2$ and O_2^- under solar irradiation. The apparent quantum yields of $^1O_2$ generation by dissolved BC were higher than many well-studied DOM, indicating that it is a highly photoactive components in the DOM pool. The ROS generated by DOM is known to mediate the indirect photolysis of many organic contaminants as well as the redox reactions of metals.[48,49] Thus, the photochemistry of dissolved BC will have considerable implications on the environmental fate of organic contaminants as well as the speciation of metals in aquatic systems with high dissolved BC concentrations. Biochar applications in agriculture and subsequent BC leaching may lead to changes in the photoreactions of contaminants and likely their adverse impacts in the flooded fields and receiving aquatic systems. Our results also indicate that phototransformation/mineralization could be an important pathway for dissolved BC losses from surface waters and oceans. We speculate that phototransformation makes dissolved BC more susceptible to biotic and abiotic degradation processes owing to the decreased aromaticity and methyl groups. The aforementioned photochemical processes of dissolved BC, namely ROS generation and phototransformation, are intertwined. Reactions with self-generated ROS was proven to be an important phototransformation mechanism. Nevertheless, phototransformation of dissolved BC reduced its ability to further generate ROS mainly due to decreased light absorption. Thus, its role in the long term photoactivity of DOM still needs further investigation.

■ ASSOCIATED CONTENT

Supporting Information

The Supporting Information is available free of charge on the ACS Publications website at DOI: 10.1021/acs.est.5b04314.

The experimental setup for irradiation experiments and the spectra of the xenon lamp and natural sunlight; E_2/E_3 ratio, spectral slopes calculated for the range of 275−295 nm, spectral slopes calculated for the range of 350−400 nm, slope ratio (S_R), $E4/E6$ ratio, TOC of dissolved BC as a function of irradiation time, the production of $^1O_2$ by Suwannee River humic acid, the UV−vis spectra of altered dissolved BC, the charge transfer spectrum, summary of experimental conditions for photochemistry experiments, the composition of the minerals in dissolved BC, and the calculation of the steady-state concentration and apparent quantum yield of $^1O_2$ (PDF)

■ AUTHOR INFORMATION

Corresponding Author

*Phone: +86-025-8968-0256; email: xiaoleiqu@nju.edu.cn (X.Q.).

Notes

The authors declare no competing financial interest.

■ ACKNOWLEDGMENTS

This work was supported by the National Natural Science Foundation of China (Grant 21407073), the National Key Basic Research Program of China (Grant 2014CB441103), China National Funds for Distinguished Young Scientists (Grant 21225729), and the Fundamental Research Funds for the Central Universities (Grant 20620140477). We thank the State Key Laboratory of Environmental Chemistry and Ecotoxicology, Research Center for Eco-Environmental Sciences, Chinese Academy of Sciences, for partial funding.

■ REFERENCES

(1) Woolf, D.; Amonette, J. E.; Street-Perrott, F. A.; Lehmann, J.; Joseph, S. Sustainable biochar to mitigate global climate change. *Nat. Commun.* **2010**, *1*, 56.
(2) Masiello, C. A. New directions in black carbon organic geochemistry. *Mar. Chem.* **2004**, *92*, 201−213.
(3) Jaffe, R.; Ding, Y.; Niggemann, J.; Vahatalo, A. V.; Stubbins, A.; Spencer, R. G. M.; Campbell, J.; Dittmar, T. Global charcoal mobilization from soils via dissolution and riverine transport to the oceans. *Science* **2013**, *340*, 345−347.
(4) Mannino, A.; Harvey, H. R. Black carbon in estuarine and coastal ocean dissolved organic matter. *Limnol. Oceanogr.* **2004**, *49*, 735−740.
(5) Dittmar, T.; Paeng, J. A heat-induced molecular signature in marine dissolved organic matter. *Nat. Geosci.* **2009**, *2*, 175−179.
(6) Zafiriou, O. C.; Joussot-Dubien, J.; Zepp, R. G.; Zika, R. G. Photochemistry of natural waters. *Environ. Sci. Technol.* **1984**, *18*, 358A−371A.
(7) Stubbins, A.; Spencer, R. G. M.; Chen, H. M.; Hatcher, P. G.; Mopper, K.; Hernes, P. J.; Mwamba, V. L.; Mangangu, A. M.; Wabakanghanzi, J. N.; Six, J. Illuminated darkness: Molecular signatures of congo river dissolved organic matter and its photochemical alteration as revealed by ultrahigh precision mass spectrometry. *Limnol. Oceanogr.* **2010**, *55*, 1467−1477.
(8) Stubbins, A.; Niggemann, J.; Dittmar, T. Photo-lability of deep ocean dissolved black carbon. *Biogeosciences* **2012**, *9*, 1661−1670.
(9) Ward, C. P.; Sleighter, R. L.; Hatcher, P. G.; Cory, R. M. Insights into the complete and partial photooxidation of black carbon in surface waters. *Environ. Sci.-Process Impacts* **2014**, *16*, 721−731.
(10) Chen, H.; Abdulla, H. A. N.; Sanders, R. L.; Myneni, S. C. B.; Mopper, K.; Hatcher, P. G. Production of black carbon-like and aliphatic molecules from terrestrial dissolved organic matter in the presence of sunlight and iron. *Environ. Sci. Technol. Lett.* **2014**, *1*, 399−404.
(11) Latch, D. E.; Stender, B. L.; Packer, J. L.; Arnold, W. A.; McNeill, K. Photochemical fate of pharmaceuticals in the environment: Cimetidine and ranitidine. *Environ. Sci. Technol.* **2003**, *37*, 3342−3350.
(12) Kujawinski, E. B.; Del Vecchio, R.; Blough, N. V.; Klein, G. C.; Marshall, A. G. Probing molecular-level transformations of dissolved organic matter: Insights on photochemical degradation and protozoan modification of dom from electrospray ionization fourier transform ion cyclotron resonance mass spectrometry. *Mar. Chem.* **2004**, *92*, 23−37.
(13) Cory, R. M.; Cotner, J. B.; McNeill, K. Quantifying interactions between singlet oxygen and aquatic fulvic acids. *Environ. Sci. Technol.* **2009**, *43*, 718−723.
(14) Qu, X.; Fu, H.; Mao, J.; Ran, Y.; Zhang, D.; Zhu, D. Chemical and structural properties of dissolved black carbon released from biochars. *Carbon* **2016**, *96*, 759−767.
(15) Chun, Y.; Sheng, G. Y.; Chiou, C. T.; Xing, B. S. Compositions and sorptive properties of crop residue-derived chars. *Environ. Sci. Technol.* **2004**, *38*, 4649−4655.
(16) Chen, D.; He, Z. Q.; Weavers, L. K.; Chin, Y. P.; Walker, H. W.; Hatcher, P. G. Sonochemical reactions of dissolved organic matter. *Res. Chem. Intermed.* **2004**, *30*, 735−753.

DOI: 10.1021/acs.est.5b04314
Environ. Sci. Technol. 2016, 50, 1218−1226

(17) Tinnacher, R. M.; Honeyman, B. D. A new method to radiolabel natural organic matter by chemical reduction with tritiated sodium borohydride. *Environ. Sci. Technol.* **2007**, *41*, 6776−6782.
(18) Sharpless, C. M. Lifetimes of triplet dissolved natural organic matter (DOM) and the effect of nabh4 reduction on singlet oxygen quantum yields: Implications for DOM photophysics. *Environ. Sci. Technol.* **2012**, *46*, 4466−4473.
(19) Hulstrom, R.; Bird, R.; Riordan, C. Spectral solar irradiance data sets for selected terrestrial conditions. *Sol. Cells* **1985**, *15*, 365−391.
(20) Haag, W. R.; Hoigne, J.; Gassman, E.; Braun, A. M. Singlet oxygen in surface waters.1. Furfuryl alcohol as a trapping agent. *Chemosphere* **1984**, *13*, 631−640.
(21) Qu, X. L.; Alvarez, P. J. J.; Li, Q. L. Photochemical transformation of carboxylated multiwalled carbon nanotubes: Role of reactive oxygen species. *Environ. Sci. Technol.* **2013**, *47*, 14080−14088.
(22) Dalrymple, R. M.; Carfagno, A. K.; Sharpless, C. M. Correlations between dissolved organic matter optical properties and quantum yields of singlet oxygen and hydrogen peroxide. *Environ. Sci. Technol.* **2010**, *44*, 5824−5829.
(23) Chen, C. Y.; Jafvert, C. T. The role of surface functionalization in the solar light-induced production of reactive oxygen species by single-walled carbon nanotubes in water. *Carbon* **2011**, *49*, 5099−5106.
(24) Sutherland, M. W.; Learmonth, B. A. The tetrazolium dyes MTS and XTT provide new quantitative assays for superoxide and superoxide dismutase. *Free Radical Res.* **1997**, *27*, 283−289.
(25) Badr, Y.; El-Wahed, M. G. A.; Mahmoud, M. A. Photocatalytic degradation of methyl red dye by silica nanoparticles. *J. Hazard. Mater.* **2008**, *154*, 245−253.
(26) Helms, J. R.; Stubbins, A.; Ritchie, J. D.; Minor, E. C.; Kieber, D. J.; Mopper, K. Absorption spectral slopes and slope ratios as indicators of molecular weight, source, and photobleaching of chromophoric dissolved organic matter. *Limnol. Oceanogr.* **2008**, *53*, 955−969.
(27) Mao, J. D.; Schmidt-Rohr, K. Accurate quantification of aromaticity and nonprotonated aromatic carbon fraction in natural organic matter by C-13 solid-state nuclear magnetic resonance. *Environ. Sci. Technol.* **2004**, *38*, 2680−2684.
(28) Johnson, R. L.; Schmidt-Rohr, K. Quantitative solid-state C-13 NMR with signal enhancement by multiple cross polarization. *J. Magn. Reson.* **2014**, *239*, 44−49.
(29) Sharpless, C. M.; Aeschbacher, M.; Page, S. E.; Wenk, J.; Sander, M.; McNeill, K. Photooxidation-induced changes in optical, electrochemical, and photochemical properties of humic substances. *Environ. Sci. Technol.* **2014**, *48*, 2688−2696.
(30) Peuravuori, J.; Pihlaja, K. Molecular size distribution and spectroscopic properties of aquatic humic substances. *Anal. Chim. Acta* **1997**, *337*, 133−149.
(31) Helms, J. R.; Mao, J. D.; Stubbins, A.; Schmidt-Rohr, K.; Spencer, R. G. M.; Hernes, P. J.; Mopper, K. Loss of optical and molecular indicators of terrigenous dissolved organic matter during long-term photobleaching. *Aquat. Sci.* **2014**, *76*, 353−373.
(32) Chin, Y.-P.; Aiken, G.; O'Loughlin, E. Molecular weight, polydispersity, and spectroscopic properties of aquatic humic substances. *Environ. Sci. Technol.* **1994**, *28*, 1853−1858.
(33) Chen, W.; Westerhoff, P.; Leenheer, J. A.; Booksh, K. Fluorescence excitation - emission matrix regional integration to quantify spectra for dissolved organic matter. *Environ. Sci. Technol.* **2003**, *37*, 5701−5710.
(34) Winter, A. R.; Fish, T. A. E.; Playle, R. C.; Smith, D. S.; Curtis, P. J. Photodegradation of natural organic matter from diverse freshwater sources. *Aquat. Toxicol.* **2007**, *84*, 215−222.
(35) Mao, J. D.; Hu, W. G.; Schmidt-Rohr, K.; Davies, G.; Ghabbour, E. A.; Xing, B. S. Quantitative characterization of humic substances by solid-state carbon-13 nuclear magnetic resonance. *Soil Sci. Soc. Am. J.* **2000**, *64*, 873−884.
(36) Sun, H. Y.; Shi, X.; Mao, J. D.; Zhu, D. Q. Tetracycline sorption to coal and soil humic acids: An examination of humic structural heterogeneity. *Environ. Toxicol. Chem.* **2010**, *29*, 1934−1942.
(37) Rossel, P. E.; Vahatalo, A. V.; Witt, M.; Dittmar, T. Molecular composition of dissolved organic matter from a wetland plant (Juncus effusus) after photochemical and microbial decomposition (1.25 yr): Common features with deep sea dissolved organic matter. *Org. Geochem.* **2013**, *60*, 62−71.
(38) Del Vecchio, R.; Blough, N. V. On the origin of the optical properties of humic substances. *Environ. Sci. Technol.* **2004**, *38*, 3885−3891.
(39) Zhang, D. N.; Yan, S. W.; Song, W. H. Photochemically induced formation of reactive oxygen species (ROS) from effluent organic matter. *Environ. Sci. Technol.* **2014**, *48*, 12645−12653.
(40) Mostafa, S.; Rosario-Ortiz, F. L. Singlet oxygen formation from wastewater organic matter. *Environ. Sci. Technol.* **2013**, *47*, 8179−8186.
(41) Sharpless, C. M.; Blough, N. V. The importance of charge-transfer interactions in determining chromophoric dissolved organic matter (CDOM) optical and photochemical properties. *Environ. Sci.-Process Impacts* **2014**, *16*, 654−671.
(42) Chin, K. K.; Trevithick-Sutton, C. C.; McCallum, J.; Jockusch, S.; Turro, N. J.; Scaiano, J. C.; Foote, C. S.; Garcia-Garibay, M. A. Quantitative determination of singlet oxygen generated by excited state aromatic amino acids, proteins, and immunoglobulins. *J. Am. Chem. Soc.* **2008**, *130*, 6912−6913.
(43) Ma, J. H.; Del Vecchio, R.; Golanoski, K. S.; Boyle, E. S.; Blough, N. V. Optical properties of humic substances and CDOM: Effects of borohydride reduction. *Environ. Sci. Technol.* **2010**, *44*, 5395−5402.
(44) Garg, S.; Rose, A. L.; Waite, T. D. Photochemical production of superoxide and hydrogen peroxide from natural organic matter. *Geochim. Cosmochim. Acta* **2011**, *75*, 4310−4320.
(45) Cory, R. M.; McNeill, K.; Cotner, J. P.; Amado, A.; Purcell, J. M.; Marshall, A. G. Singlet oxygen in the coupled photochemical and biochemical oxidation of dissolved organic matter. *Environ. Sci. Technol.* **2010**, *44*, 3683−3689.
(46) Wilkinson, F.; Helman, W. P.; Ross, A. B. Rate constants for the decay and reactions of the lowest electronically excited singlet-state of molecular-oxygen in solution - an expanded and revised compilation. *J. Phys. Chem. Ref. Data* **1995**, *24*, 663−1021.
(47) Latch, D. E.; McNeill, K. Microheterogeneity of singlet oxygen distributions in irradiated humic acid solutions. *Science* **2006**, *311*, 1743−1747.
(48) Lam, M. W.; Tantuco, K.; Mabury, S. A. Photofate: A new approach in accounting for the contribution of indirect photolysis of pesticides and pharmaceuticals in surface waters. *Environ. Sci. Technol.* **2003**, *37*, 899−907.
(49) Nico, P. S.; Anastasio, C.; Zasoski, R. J. Rapid photo-oxidation of Mn(II) mediated by humic substances. *Geochim. Cosmochim. Acta* **2002**, *66*, 4047−4056.

DOI: 10.1021/acs.est.5b04314
Environ. Sci. Technol. 2016, 50, 1218−1226